

Validation of quasi-invariant ice cloud radiative quantities with MODIS satellite-based cloud property retrievals

Jiachen Ding,^{a,*} Ping Yang,^a George W. Kattawar^b
Michael D. King,^{c,a} Steven Platnick,^d Kerry G. Meyer^d

^a *Department of Atmospheric Sciences, Texas A&M University, College Station, TX 77845, USA*

^b *Department of Physics & Astronomy and Institute for Quantum Science and Engineering, Texas A&M University, College Station 77845, TX, USA*

^c *Laboratory for Atmospheric & Space Physics, University of Colorado, CO 80303, USA*

^d *Earth Sciences Division, NASA Goddard Space Flight Center, Greenbelt, MD 20771, USA*

For publication in the
Journal of Quantitative Spectroscopy and Radiative Transfer

* Corresponding author address: Jiachen Ding, Department of Atmospheric Sciences, Texas A&M University, College Station, TX 77843, USA; *E-mail address:* njudjc@tamu.edu

Abstract

Similarity relations applied to ice cloud radiance calculations are theoretically analyzed and numerically validated. If $\tau(1-\varpi)$ and $\tau(1-\varpi g)$ are conserved where τ is optical thickness, ϖ the single-scattering albedo, and g the asymmetry factor, it is possible that substantially different phase functions may give rise to similar radiances in both conservative and non-conservative scattering cases, particularly in the case of large optical thicknesses. In addition to theoretical analysis, this study uses operational ice cloud optical thickness retrievals from the Moderate Resolution Imaging Spectroradiometer (MODIS) Level 2 Collection 5 (C5) and Collection 6 (C6) cloud property products to verify radiative similarity relations. It is found that, if the MODIS C5 and C6 ice cloud optical thickness values are multiplied by their respective $(1-\varpi g)$ factors, the resultant products referred to as the effective optical thicknesses become similar with their ratio values around unity. Furthermore, the ratios of the C5 and C6 ice cloud effective optical thicknesses display an angular variation pattern similar to that of the corresponding ice cloud phase function ratios. The MODIS C5 and C6 values of ice cloud similarity parameter, defined as $[(1-\varpi)/(1-\varpi g)]^{1/2}$, also tend to be similar.

Keywords: radiative transfer, similarity relations, ice cloud property retrieval product, MODIS

1. Introduction

The similarity relations for the radiative transfer processes under different atmospheric conditions have been extensively investigated (e.g. [1-12]). In particular, van de Hulst proposed the similarity relations for the transfer of radiation (e.g. [1-4]) primarily in the case of flux calculations. For the diffuse radiation field in the deeply diffusive regime within a scattering medium such as a cloud layer, the radiance can be expressed as [2]

$$I(\tau, \mu) = c_1 h(\mu) e^{-k\tau} + c_2 h(-\mu) e^{k\tau}, \quad (1)$$

where I is the scattered radiance, τ is the optical thickness, and μ ($-1 < \mu < 1$) is the direction cosine with respect to the zenith direction. k is an eigenvalue, known as the diffusion exponent, which can be interpreted as the inverse of diffusion length. $h(\mu)$ is the eigenfunction referred to as the diffusion pattern [2]. If all $h(\mu)$ and $k\tau$ are invariant, the solution for the radiance given by Eq. (1) will be invariant as well.

The relevant multiple scattering calculations may show similar flux and radiance for two clouds if the quantities $\varpi\tau(1-g)$ and $(1-\varpi)/k$ are conserved, where g is the asymmetry factor of the phase function of a homogeneous scattering atmosphere layer and ϖ is the single-scattering albedo [3]. Sobolev [12] discussed the similarity relations between anisotropic scattering and isotropic scattering. Chandrasekhar [13] also reported a similar study in the case of conservative scattering (i.e. $\varpi=1$) [13]. van de Hulst [4] presented two simple similarity relations based on the similarity of Eq. (1) for two different scattering atmospheres. Specifically, the planetary and spherical albedo [14] may be conserved if the following two relations are satisfied:

$$\tau(1-\varpi) = \tau'(1-\varpi'), \quad (2)$$

and

$$\tau(1-\varpi g) = \tau'(1-\varpi' g'). \quad (3)$$

The difference between the above two equations [specifically, Eq. (3) minus Eq. (2)] leads to the following relation:

$$\varpi\tau(1-g)=\varpi'\tau'(1-g'). \quad (4)$$

Note that, regarding radiative transfer similarity, Eq. (3) was used by Joseph et al. [15] and Eqs. (2) and (3) are used by Twomey and Bohren [16] in their respective studies.

As pointed out by Twomey and Bohren [16], $(1-g)$ is a factor related to the average degree of deviation of scattering from the forward scattering. As an approximately invariant quantity shown by Eq. (4), the quantity $\varpi\tau(1-g)$ is referred to as the effective scattering optical thickness. Moreover, it is obvious that $\tau(1-\varpi)$ indicates the absorption optical thickness. The quantity $\tau(1-\varpi g)$, given by the sum of $\tau(1-\varpi)$ and $\varpi\tau(1-g)$, is referred to as the effective optical thickness, which is a manifestation of the fact that the extinction coefficient is the sum of the absorption coefficient and the scattering coefficient.

McKellar and Box (1981) [8] presented the condition under which the two solutions to the radiative transfer equation (RTE) with distinctly different optical thicknesses and phase functions may be identical. In addition, they explained the connections between the similarity relation proposed by van de Hulst [4] and an invariant scaling of the RTE. Previous studies, except the work by Platnick et al. [17] who discussed the ice cloud optical thickness retrieval differences arising from two different ice radiative models, focus essentially on enhancing the computational efficiency of flux, spherical albedo, and radiance computations based on similarity relations. For example, the Delta-Eddington approximation proposed by Joseph et al. [15] and the Delta-M method developed by Wiscombe [18] accelerate the flux computation. King [19] and King and Harshvardhan [20] discuss similarity relations in asymptotic theory. Iwabuchi [21] scales optical thickness, single-scattering albedo, and phase function based on the similarity relation to improve the ray-tracing efficiency in a Monte Carlo radiative transfer model. Cahalan et al. [22] show the similarity of nadir radiance computed by 3D radiative transfer models involving scaled cloud optical properties. However, the degree of similarity in radiance simulations in conjunction with two different phase functions that are strongly anisotropic (e.g., the phase functions associated with ice clouds at visible or near-infrared wavelengths), and the implications of the similarity relation in some practical applications such as remote sensing are not well quantified.

This study focuses on the analysis and validation of radiative similarity relations in the case of ice clouds by using radiative transfer modeling capabilities and satellite-based cloud property retrievals. In Section 2, the theoretical and numerical validations of the similarity relations are presented. Section 3 indirectly validates the similarity relations using remote sensing data and discusses their application in interpreting cloud property retrieval results. Section 4 summarizes and presents conclusions of this study.

2. Theoretical and numerical validation

The RTE in a plane-parallel scattering atmosphere without thermal emission is

$$\mu \frac{\partial I(\tau, \mu, \phi)}{\partial \tau} = I(\tau, \mu, \phi) - \frac{\varpi}{4\pi} \int_{-1}^1 \int_0^{2\pi} I(\tau, \mu', \phi') P(\mu, \phi; \mu', \phi') d\mu' d\phi', \quad (5)$$

where P is the phase function, ϕ and ϕ' are viewing and incident azimuth angles, and μ and μ' are viewing and incident zenith angles. Multiplying the n -th order Legendre polynomial $p_n(\mu)$ and integrating with respect to μ and ϕ on both sides of Eq. (5), we obtain

$$\begin{aligned} \int_{-1}^1 \int_0^{2\pi} \mu \frac{\partial I(\tau, \mu, \phi)}{\partial \tau} p_n(\mu) d\mu d\phi &= \int_{-1}^1 \int_0^{2\pi} I(\tau, \mu, \phi) p_n(\mu) d\mu d\phi \\ &- \frac{\varpi}{4\pi} \int_{-1}^1 \int_0^{2\pi} \int_{-1}^1 \int_0^{2\pi} I(\tau, \mu', \phi') P(\mu, \phi; \mu', \phi') p_n(\mu) d\mu' d\phi' d\mu d\phi. \end{aligned} \quad (6)$$

According to the addition theorem of spherical harmonics, the phase function can be expanded as

$$P(\mu, \phi; \mu', \phi') = \sum_{n=0}^{\infty} \sum_{m=0}^{\infty} \frac{(n-m)!}{(n+m)!} (2 - \delta_{m0}) C_n p_n^m(\mu) p_n^m(\mu') \cos m(\phi - \phi'), \quad (7)$$

where δ_{m0} is the Kronecker delta, p_n^m is the associated Legendre polynomial, and C_n is the expansion coefficient. Utilizing the orthogonality of the cosine function and Legendre polynomial, from Eqs. (6) and (7), we obtain

$$\int_{-1}^1 \int_0^{2\pi} \mu \frac{\partial I(\tau, \mu, \phi)}{\partial \tau} p_n(\mu) d\mu d\phi = \left(1 - \frac{\varpi C_n}{2n+1}\right) \int_{-1}^1 \int_0^{2\pi} I(\tau, \mu, \phi) p_n(\mu) d\mu d\phi. \quad (8)$$

For a different atmosphere, Eq. (8) can be given, with relevant radiative quantities denoted by prime symbols, in the form:

$$\int_{-1}^1 \int_0^{2\pi} \mu \frac{\partial I'(\tau', \mu, \phi)}{\partial \tau'} p_n(\mu) d\mu d\phi = \left(1 - \frac{\varpi' C'_n}{2n+1}\right) \int_{-1}^1 \int_0^{2\pi} I'(\tau', \mu, \phi) p_n(\mu) d\mu d\phi. \quad (9)$$

If $I(\tau, \mu, \phi)$ and $I'(\tau', \mu, \phi)$ in Eqs. (8) and (9) are equal, it follows from Eqs. (8) and (9) that we must have the following relation:

$$\frac{\tau'}{\tau} = \frac{2n+1-\varpi C_n}{2n+1-\varpi' C'_n}, \quad (10)$$

which can be rearranged in the form

$$\tau(2n+1-\varpi C_n) = \tau'(2n+1-\varpi' C'_n). \quad (11)$$

Eq. (11) is the same as the invariant scaling condition reported by McKellar and Box [8], who used a different derivation. The cases with $n = 0$ ($C_0=1$) and $n = 1$ ($C_1=3g$) in Eq. (11) correspond to Eqs. (2) and (3), respectively. For two arbitrary phase functions, it is essentially impossible to satisfy Eq. (8) for all n . However, Eqs. (2) and (3) can be satisfied, leading to similar results in radiative transfer simulations.

In this study, the DIScrete Ordinate Radiative Transfer model (DISORT) [23] is implemented with 256 streams to compute the radiation field of a single ice cloud layer with collimated incoming solar radiation as the source. Since we focus on the scattering property of the cloud layer, the surface reflection is not considered and, thus, is set to zero in the computation. Viewing zenith angle 0° is defined as upward so the downward normal direction is 180° . The Moderate Resolution Imaging Spectroradiometer (MODIS) Collection 5 (C5) and Collection 6 (C6) ice cloud optical property models are used in the calculations. The C5 ice cloud model is a mixture of multiple ice particle habits [24] and the C6 model represents all ice particles as severely-roughened aggregated hexagonal columns [17, 25]. The phase functions of the C5 and C6 models in MODIS spectral band 2 ($0.86 \mu m$ central wavelength) and band 7 ($2.13 \mu m$ central wavelength) are shown in Fig. 1 for an effective particle radius of $30 \mu m$. Obviously, the C5 and C6 phase functions are quite different. The C5 phase function has apparent peaks in both the forward and backward

scattering directions, whereas the C6 phase function is much smoother. The corresponding single-scattering albedos and asymmetry factors of the C5 and C6 models are shown in Fig. 2. In band 7, their single-scattering albedos are different, particularly for large sizes. The asymmetry factors of the C5 phase functions are larger than C6 in corresponding bands except for quite small particles. The following numerical results will show that even though the C5 and C6 models are different, the radiative transfer computations with the two models may give similar results if Eqs. (2) and (3) are satisfied.

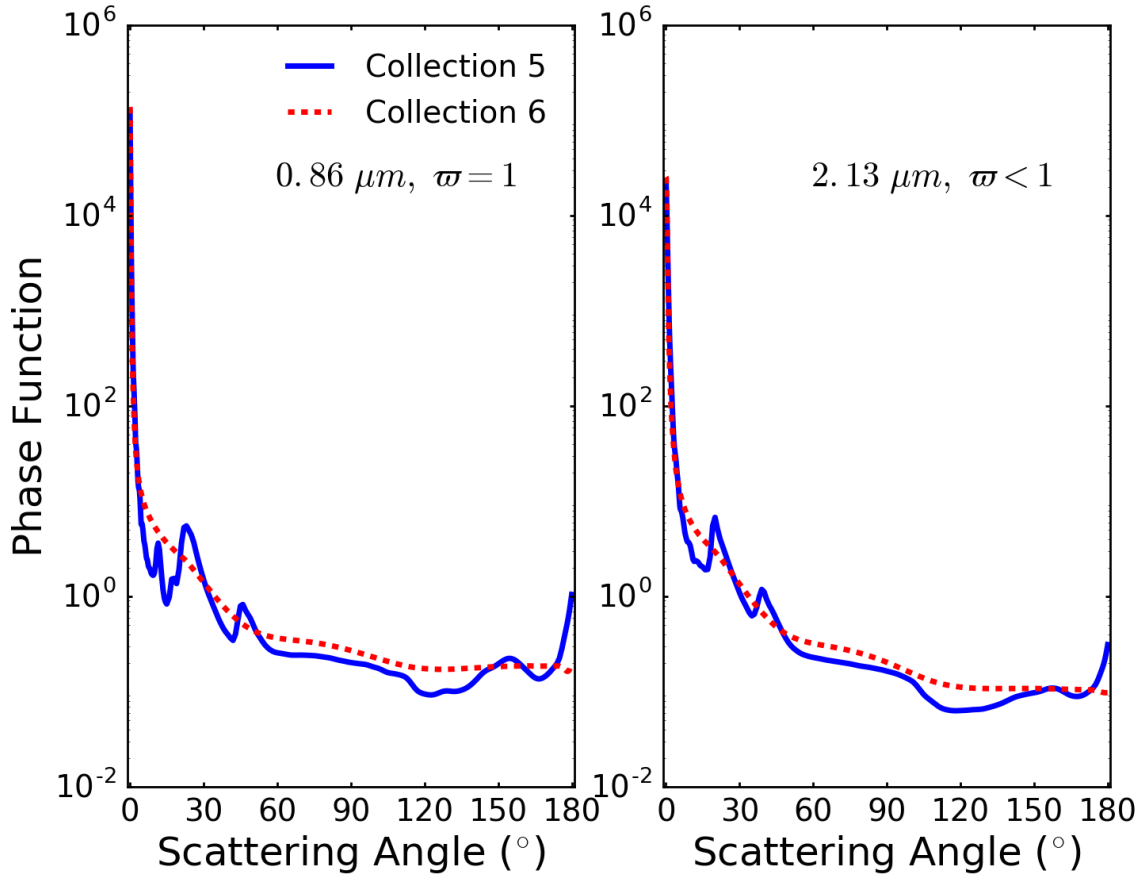


Fig. 1. Phase functions of the MODIS C5 and C6 ice cloud models in MODIS band 2 ($0.86 \mu m$) and 7 ($2.13 \mu m$) with effective radius $30 \mu m$.

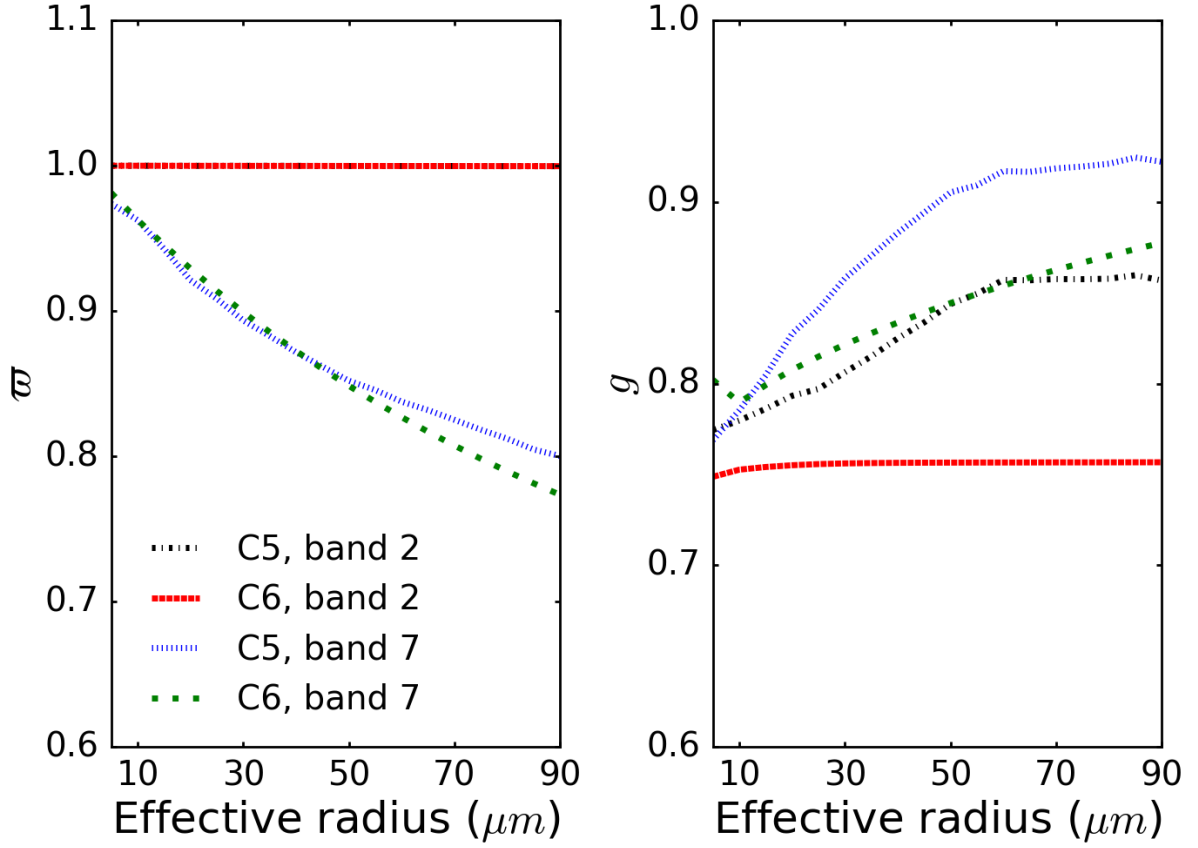


Fig. 2. The single-scattering albedo ϖ (left panel) and asymmetry factor g (right panel) as a function of effective radius of the MODIS C5 and C6 ice cloud models in MODIS bands 2 and 7.

In the present radiative transfer computations, the effective optical thickness $\tau(1-\varpi g)$ and absorption optical thickness $\tau(1-\varpi)$ are conserved but optical thickness τ is different for the C5 and C6 models because they have different asymmetry factors and/or single-scattering albedos, as illustrated in Fig. 2. In MODIS band 2, the ice cloud does not absorb light ($\varpi = 1$). Thus, the calculation in band 2 is equivalent to assuming $\tau(1-g)$ invariant, and Eq. (2) is automatically satisfied since ϖ is essentially unity for both the C5 and C6 models. Ice cloud is absorptive in band 7 ($\varpi < 1$) so both τ and ϖ should be scaled to satisfy Eqs. (2) and (3) concurrently, which suggests that the quantity

$$s \equiv \sqrt{\frac{1-\varpi}{1-\varpi g}}, \quad (12)$$

is conserved. s is referred to as the similarity parameter, following van de Hulst [4]. The single-scattering albedo of the C5 model in band 7 is scaled by keeping s invariant.

Fig. 3 shows the simulated reflectance for ice cloud particle effective radius $30 \mu m$, effective optical thickness $\tau(1-\varpi_g)=4$ ($\tau \cong 16$), solar zenith angle 20° , and relative azimuth angle 0° . Although the two phase functions are different, the reflectance calculation results are similar if Eqs. (2) and (3) are satisfied, and the relative differences are less than 8% for most viewing zenith angles in the case of large optical thickness ($\tau > 2$). For other solar zenith angles and relative azimuth angles, the relative differences are also smaller than 8% for most viewing zenith angles, except in the case of grazing incidence (near 90°) where the reflectance is dominated by single scattering.

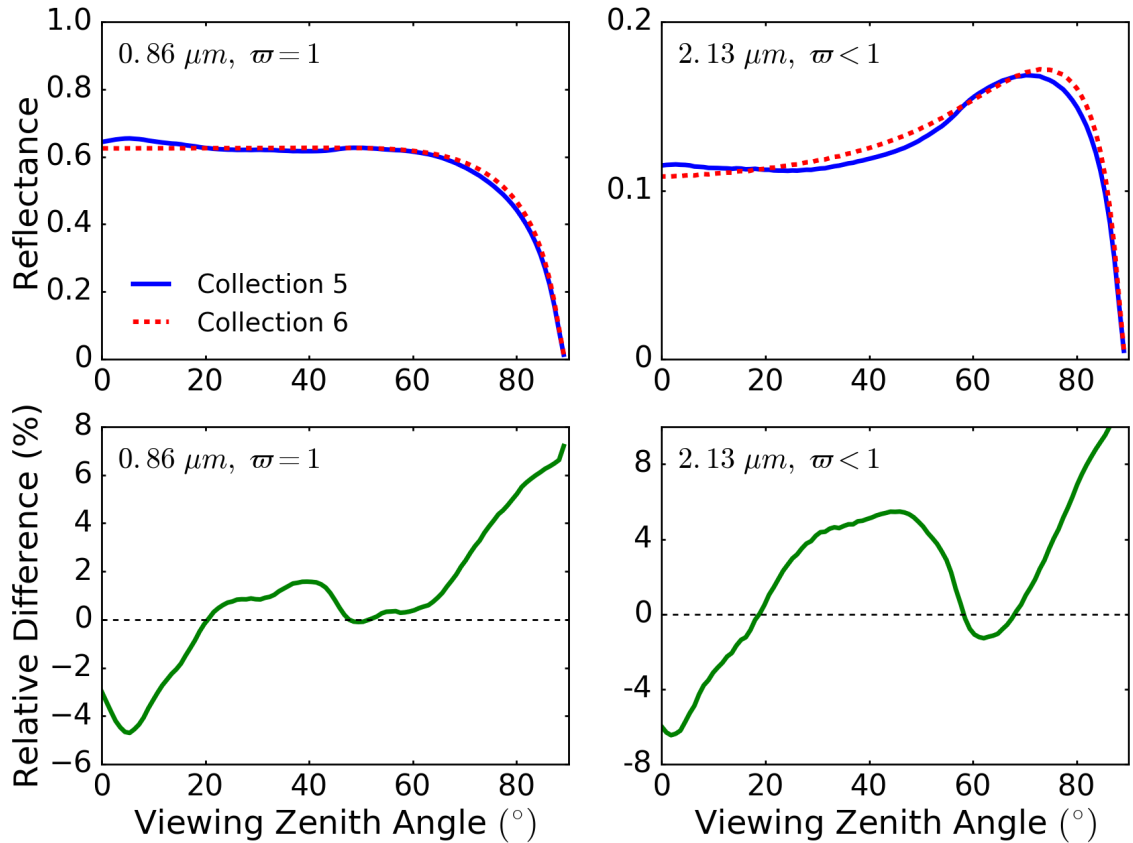


Fig. 3. Reflectance (upper row) and relative difference (lower, C6-C5 percentage difference) calculated based on the C5 and C6 ice cloud models with Eqs. (2) and (3) satisfied. The solar zenith angle is 20° , and relative azimuth angle is 0° . The ice clouds have effective radius $30 \mu m$, and the effective optical thickness $\tau(1-\varpi_g)$ is 4. **Left columns:** MODIS band 2; **Right column:**

The transmittance calculation results for the same settings as the reflectance calculation are shown in Fig. 4. Except in the forward scattering directions (around viewing zenith angle 160°), the transmittance results are similar. The similar error levels are also seen in other solar zenith angles and relative azimuth angles. The large differences in forward scattering directions are partly due to the limitation of the DISORT code. In DISORT, the TMS [26] method is used to correct the single scattering calculation, which makes the radiative transfer calculation more accurate in other scattering directions but introduces a large bias in forward scattering directions [27].

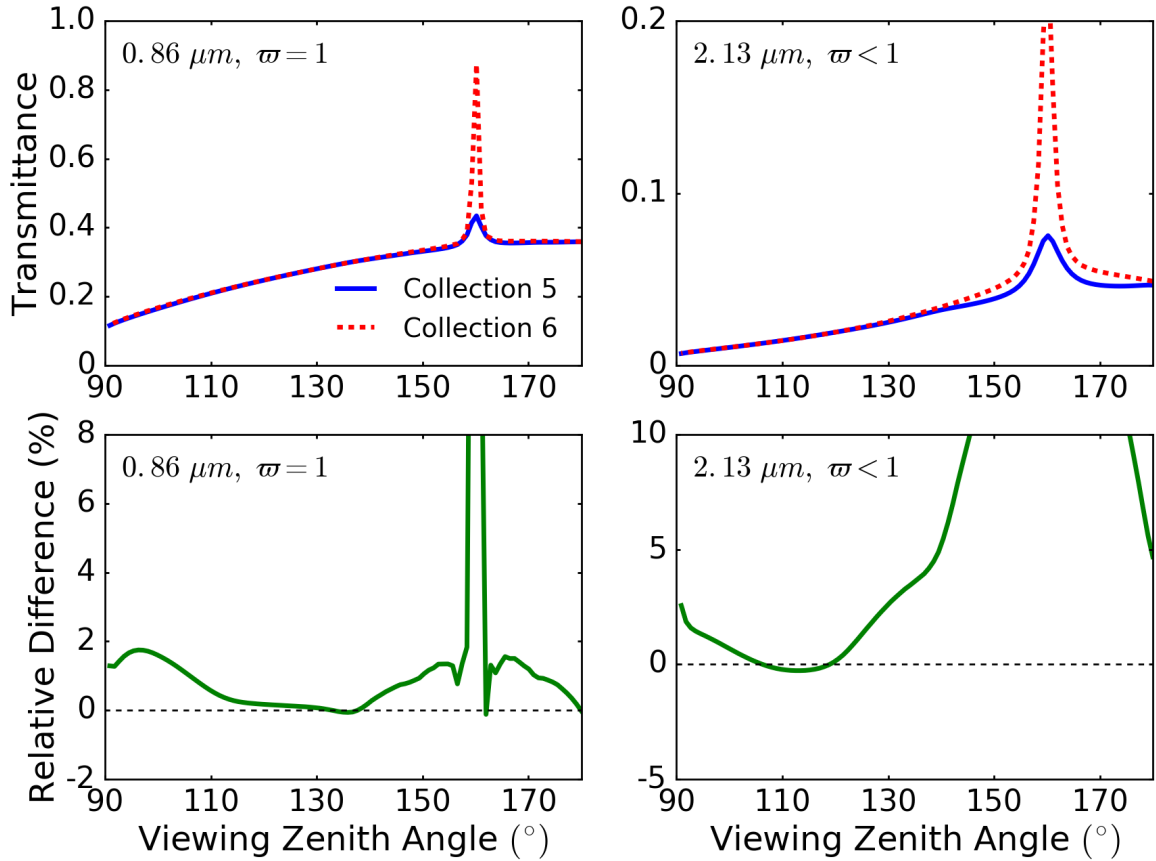


Fig. 4. Transmittance (upper) and relative difference (C6-C5 percentage difference, lower) calculated based on the C5 and C6 ice cloud models and with Eqs. (2) and (3) satisfied. The solar zenith angle is 20° , and relative azimuth angle is 0° . The ice clouds have effective radius $30 \mu\text{m}$, and the effective optical thickness $\tau(1-\varpi_g)$ is 4. **Left columns:** MODIS band 2; **Right column:** MODIS band 7.

The similarity also depends on optical thickness. Fig. 5 compares the C6/C5 phase function ratio and the C6/C5 reflectance ratio with various effective optical thickness $\tau(1-\omega_g)$. For small effective optical thickness (e.g., 0.01 in Fig. 5), the reflectance ratio patterns are similar to the phase function ratio pattern because single scattering dominates the reflectance for optically thin clouds. As the effective optical thickness increases, the reflectance ratio curves become smooth, and in fact converge when the effective optical thickness is 2 ($\tau \cong 10$) or greater.

For large effective optical thickness, in the case of conservative scattering (band 2), the C6/C5 reflectance ratio is nearly unity and tends to be independent of scattering angle whereas in the case of non-conservative scattering (band 7), the ratio still shows an angular dependence. For non-conservative scattering, the total energy of scattered light will decrease due to absorption each time a scattering occurs so that only low-order scattering events contribute to the reflected light, which has stronger angular dependence. In contrast, for conservative scattering, high-order scattering events contribute comparably to the reflected radiation, which results in more isotropic reflectance.

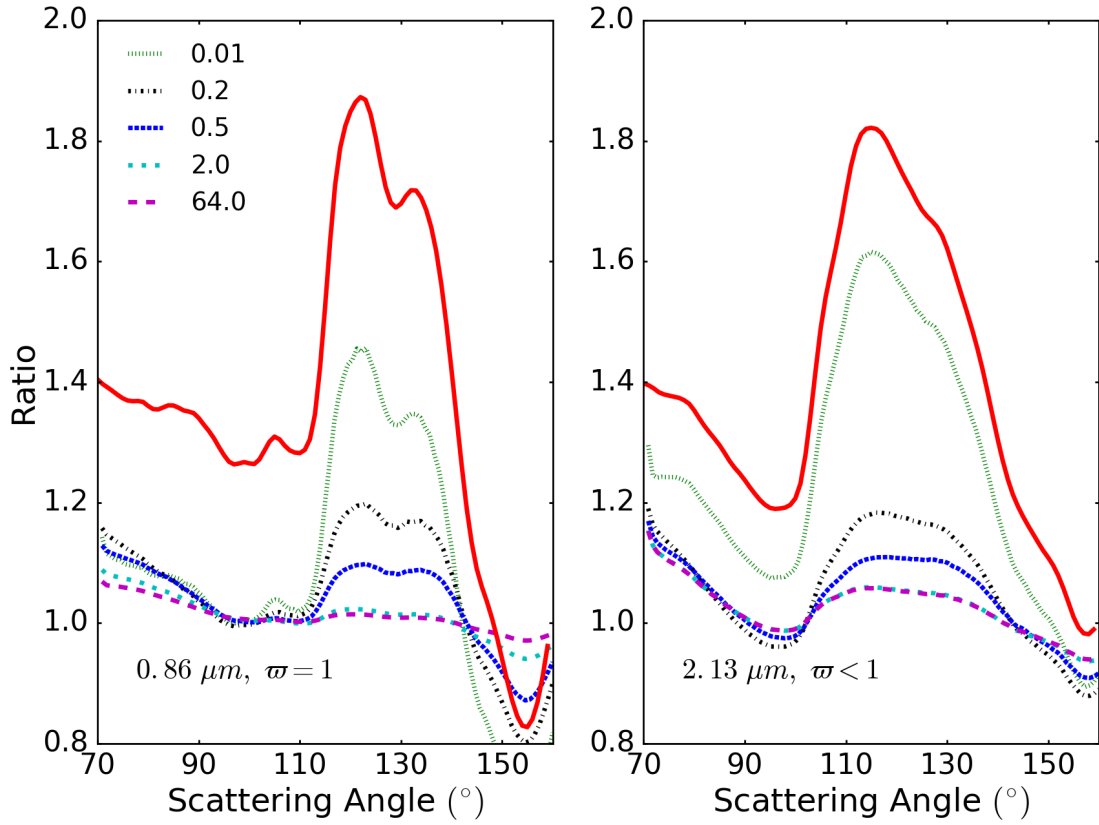


Fig. 5. The solid red curves are the C6/C5 phase function ratios in MODIS bands 2 (left panel) and 7 (right panel). The dotted and dashed curves are C6/C5 reflectance ratios for various effective optical thicknesses. Colors and line styles represent different $\tau(1-\omega_g)$ values listed in the left plot.

Fig. 6 compares simulated ice cloud reflectivity in MODIS band 2 with 10000 randomly sampled MODIS viewing geometries and optical thicknesses (solar and sensor-viewing zenith angles are sampled between 0° and 60° , relative azimuth angles are sampled between 0° and 180° , and ice cloud optical thicknesses are sampled between 0.001 and 10) based on the C5 and C6 ice cloud optical property models. If the optical thickness τ is conserved, the band 2 reflectivity based on the C6 ice model ($R_{2,C6}$) is apparently larger than that based on the C5 ice model ($R_{2,C5}$), as shown in the left panel of Fig. 6. If the effective optical thickness $\tau(1-\omega_g)$ is conserved, $R_{2,C5}$ and $R_{2,C6}$ are almost identical, as shown in the right panel of Fig. 6. Because the C6 ice model gives a smaller asymmetry factor than the C5 ice model in band 2 (see Fig. 2), the same reflectivity in band 2 corresponds to smaller optical thickness if the C6 model, rather than C5, is used in the calculation in comparison.

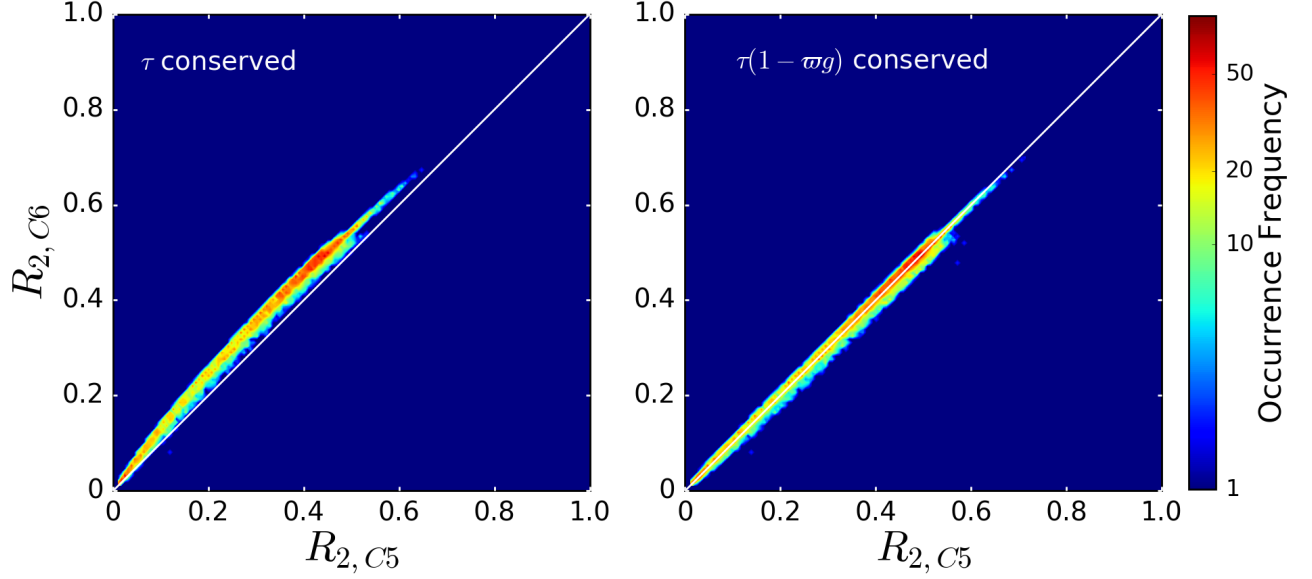


Fig. 6. The comparison of MODIS band 2 reflectivity calculated based on the C5 and C6 ice cloud models. **Left:** with the same optical thickness τ ; **Right:** with the same effective optical thickness $\tau(1 - \omega g)$. The occurrence frequency has a logarithmic scale, and represents the number of data points in each bin.

Fig. 7 compares simulated ice cloud reflectivity in MODIS band 7 with the same viewing geometry and optical thicknesses as Fig. 6. Four groups of calculation are carried out based on the C5 and C6 ice cloud models in band 7. The four groups are, conserving τ , satisfying only Eq. (2), satisfying only Eq. (3), and satisfying both Eqs. (2) and (3) (i.e. keeping s invariant). If τ is conserved, the band 7 reflectivity based on the C6 model ($R_{7,C6}$) is larger than that based on the C5 model ($R_{7,C5}$) since the asymmetry factor of C6 is smaller than C5 as shown in Fig. 2. Though one of the similarity relations (Eqs. (2) and (3)) is satisfied, as shown in Fig. 7(b, c), $R_{7,C6}$ is still larger than $R_{7,C5}$. Only if both Eqs. (2) and (3) are satisfied, which implies the similarity parameter s is invariant, $R_{7,C6}$ and $R_{7,C5}$ are almost identical as shown in Fig. 7(d). The implications of the radiative characteristics shown in Figs. 6 and 7 will be further illustrated in section 3 from the perspective of retrieving ice cloud optical thickness and effective particle size.

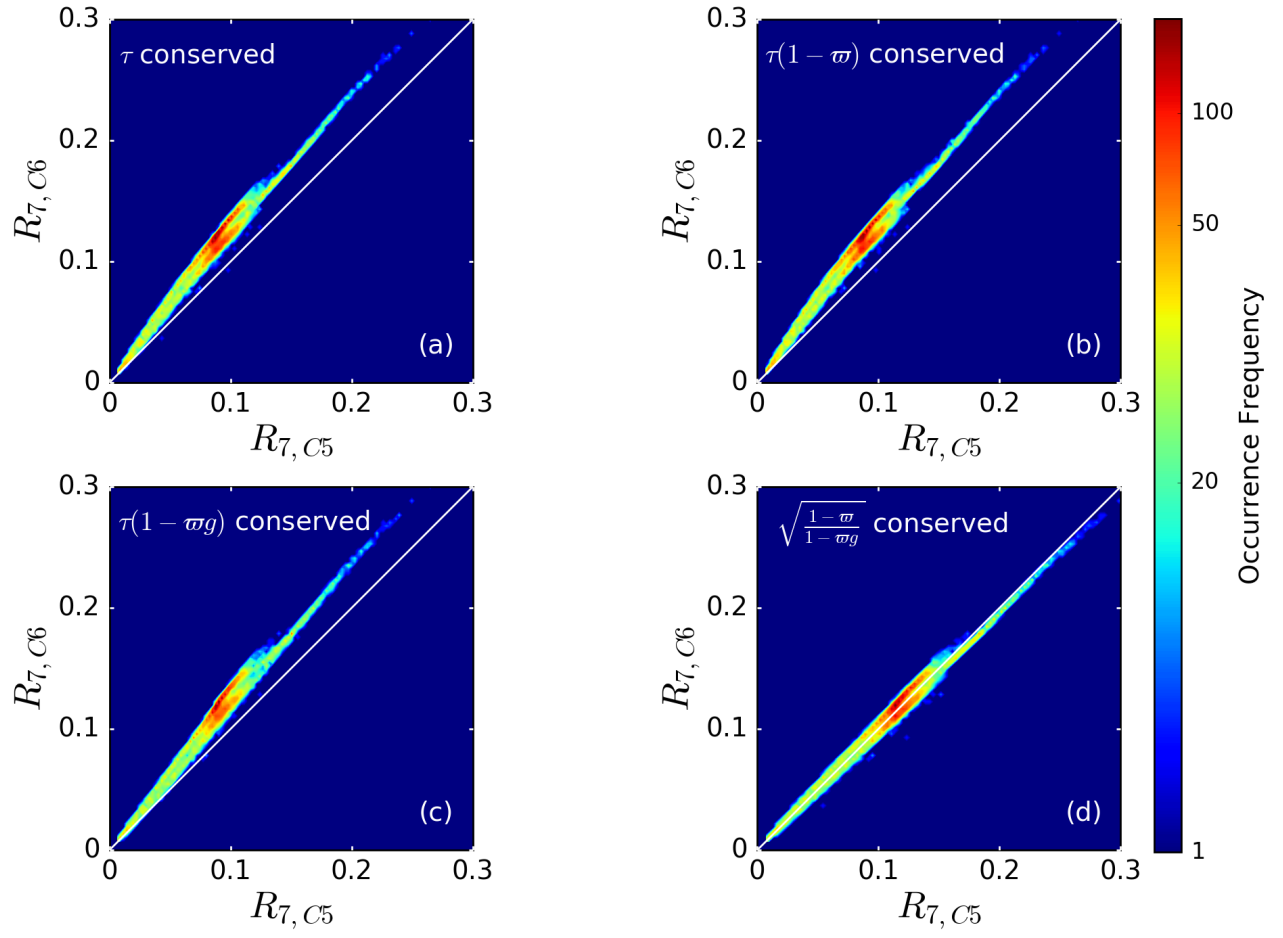


Fig. 7. The comparison of MODIS band 7 reflectivity calculated based on the C5 and C6 ice cloud models. **(a):** with the same optical thickness τ ; **(b):** with the same absorption optical thickness $\tau(1-\omega)$; **(c):** with the same effective optical thickness $\tau(1-\omega g)$; **(d):** with the same similarity parameter s . The occurrence frequency has a logarithmic scale, and represents the number of data points in each bin.

3. Validation using remote sensing data

In this section, the MODIS operationally retrieved ice cloud optical property datasets based on the C5 and C6 ice cloud models are used to validate the above analysis of the similarity conditions. For these operational products, ice cloud optical thickness and effective radius are retrieved simultaneously from MODIS Level 1B reflectance data with a bi-spectral-band retrieval algorithm [28]. The C5 and C6 ice cloud models described above are used to compute the Look-up Tables (LUTs) in the operational MODIS retrieval implementation. The Level 1B reflectance data used in C5 and C6 cloud optical property re-

trievals are slightly different due to updated reflective solar bands calibration implemented in the C6 product [29]. In the granule used in the study, band 2 and 7 reflectance differences between C5 and C6 data are less than 0.001, so the retrieved C5 and C6 ice cloud optical properties can be assumed to correspond to the same radiation field.

A. Data

The optical property data are from one granule of Aqua MODIS Level 2 C5 and C6 cloud products located over the North Pacific Ocean [30], where an ocean surface is assumed in all retrievals. The left panel of Fig. 8 shows the true color RGB image of the 5 minuts granule obtained on May 25, 2016, which corresponds to 2000 km along track and 2330 km cross track, and is located between about 30° N to 50° N latitude, and from about 160° E to 165° W longitude. The technical details of the operational MODIS cloud property retrieval products, forward light scattering, and radiative transfer simulations involved in implementing the MODIS cloud optical property retrieval algorithm are reported by Platnick et al. [17]. Over 50% of the pixels in the granule are classified as ice clouds according to the cloud phase (optical properties) in both the C5 and C6 cloud products. Over ocean, MODIS bands 2 and 7 are used for the cloud optical property retrievals.

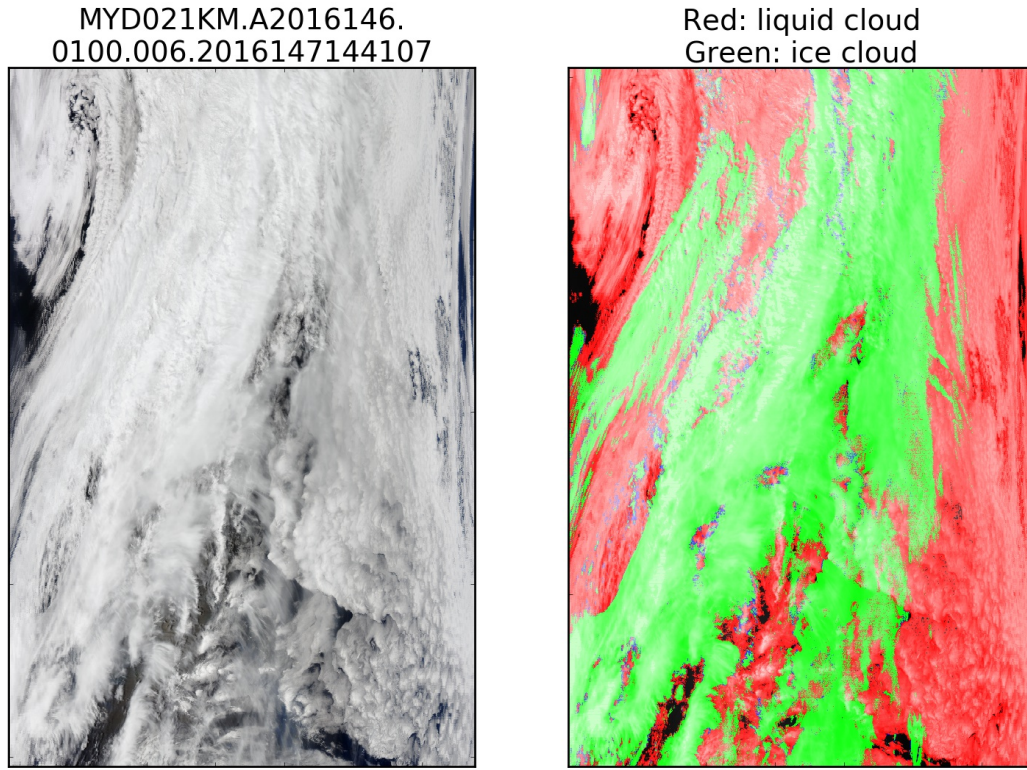


Fig. 8. Left: RGB image of Aqua MODIS Level 1B reflectance data (MYD021KM.A2016146.0100.006.2016147144107)
Right: Distribution of cloud phases (from MODIS C6 Level 2 data) in the granule.

B. Results and analysis

Fig. 9 compares the operational MODIS C5 and C6 ice cloud optical thicknesses (at $0.67 \mu m$ wavelength). Only the pixels that are classified as ice clouds over ocean by both the C5 and C6 cloud phase flags are included in the comparison. Note that the cloud phase flags used here are named “Cloud_Phase_Optical_Properties” in both MODIS Level 2 cloud products, and are used in optical thickness and effective radius retrievals. In addition, QA flags are used to filter out pixels with clear sky restoral. Obviously, the C6 ice cloud optical thickness is smaller than C5, but they have a nearly linear relationship. The difference of the C5 and C6 ice cloud optical thickness is consistent with the $R_{2,C5}$ and $R_{2,C6}$ differences shown in the left panel of Fig. 6. For optical thicknesses larger than 15, two data branches occur in the relation.

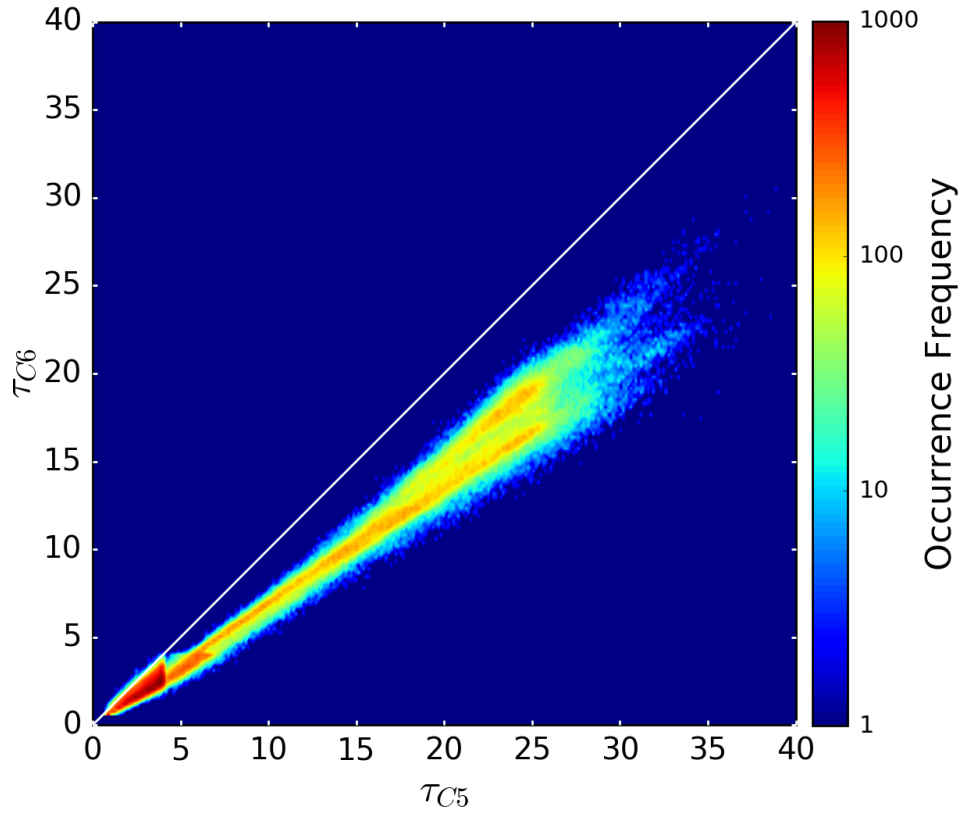


Fig. 9. Comparison of C5 and C6 ice cloud optical thickness at $0.67 \mu m$ wavelength. The white straight line is the one-to-one ratio line. The occurrence frequency has a logarithmic scale, and represents the number of data points in each bin.

Fig. 10 shows the relation of the scaled (effective) optical thickness $\tau(1-\varpi g)$ for the C5 and C6 ice cloud optical thicknesses retrieved using MODIS band 2. τ is scaled to band 1 ($0.67 \mu m$), and ϖ and g for each pixel correspond to the retrieved effective size for each pixel and the respective ice cloud model. The distribution of $\tau(1-\varpi g)$ data points is symmetrical around the one-to-one ratio line. This implies that similar $\tau(1-\varpi g)$ values can give similar radiation fields. In a bi-spectral-band retrieval algorithm, the non-absorptive band mainly determines the optical thickness [28], so the similarity of the $\tau(1-\varpi g)$ values is consistent with the analysis in Section 2. In addition, the two data branches lie on two sides of the one-to-one ratio line and the broadening of the relation is obvious. The effective optical thickness retrieved in band 1 is also conserved (not shown).

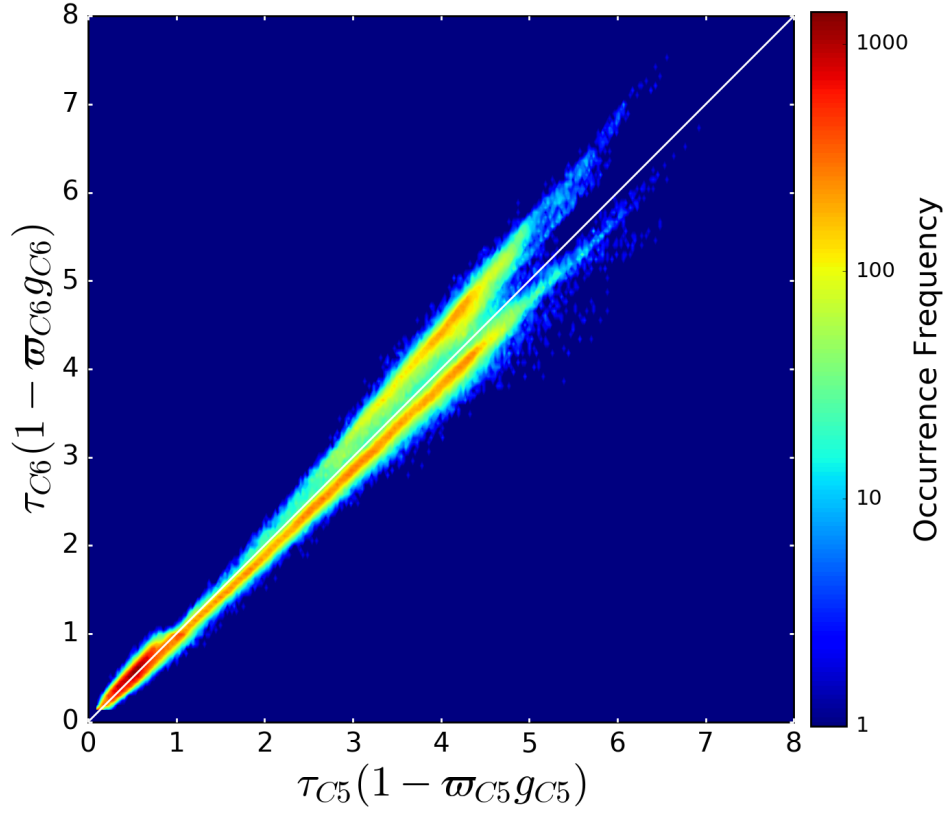


Fig. 10. Comparison of $\tau(1-\varpi g)$ for the C5 and C6 ice cloud optical thickness data in MODIS band 2. The white straight line is the one-to-one ratio line. The occurrence frequency has a logarithmic scale, and represents the number of data points in each bin.

To further investigate the angular dependence of the $\tau(1-\varpi g)$ relation between the two datasets, the C6/C5 $\tau(1-\varpi g)$ ratio is plotted in the right panel of Fig. 11. The C6/C5 $\tau(1-\varpi g)$ ratio centers on unity and has nearly the same angular dependence as the C5/C6 phase function ratio in the left panel. This is due to the low-order scattering contribution, which is analyzed in Section 2. In retrievals, the observed reflectance is compared with the computed reflectance to obtain effective optical thickness. Therefore, the C6/C5 effective optical thickness ratio also has a similar angular dependence as the C5/C6 phase function ratio. The angular dependence can also explain the two data branches shown in Figs. 9 and 10. Fig. 12 shows the viewing geometry and scattering angle distributions of the two data branches for effective optical thicknesses larger than 3. In Fig. 12(d), upper and lower branches have obviously distinct scattering angles due to varied solar zenith angles, sensor zenith angles, and relative azimuth angles. The upper branch mostly have scattering angle $140^\circ \sim 160^\circ$ whereas the lower branch mostly have $110^\circ \sim 140^\circ$ scattering angle. The

two angle ranges coincide with the maxima and minima of the C6/C5 $\tau(1-\omega g)$ ratio, and the C5/C6 phase function ratio shown in Fig. 11.

Compared with the phase function ratio in the left panel of Fig. 11, the effective optical thickness ratio in the right panel has a smaller amplitude of variation, which is consistent with Fig. 5. The ice cloud pixels in the selected granule have moderate optical thickness, so multiple scattering events contribute to some fraction of the reflectance, which is less angularly dependent. Thus, the retrieval yields smoother effective optical thickness ratios. Moreover, Fig. 11 suggests a stricter similarity condition. If the relation between τ and τ' is defined to be angle-dependent rather than constant as in Eq. (3), the radiative transfer calculation may then be the same.

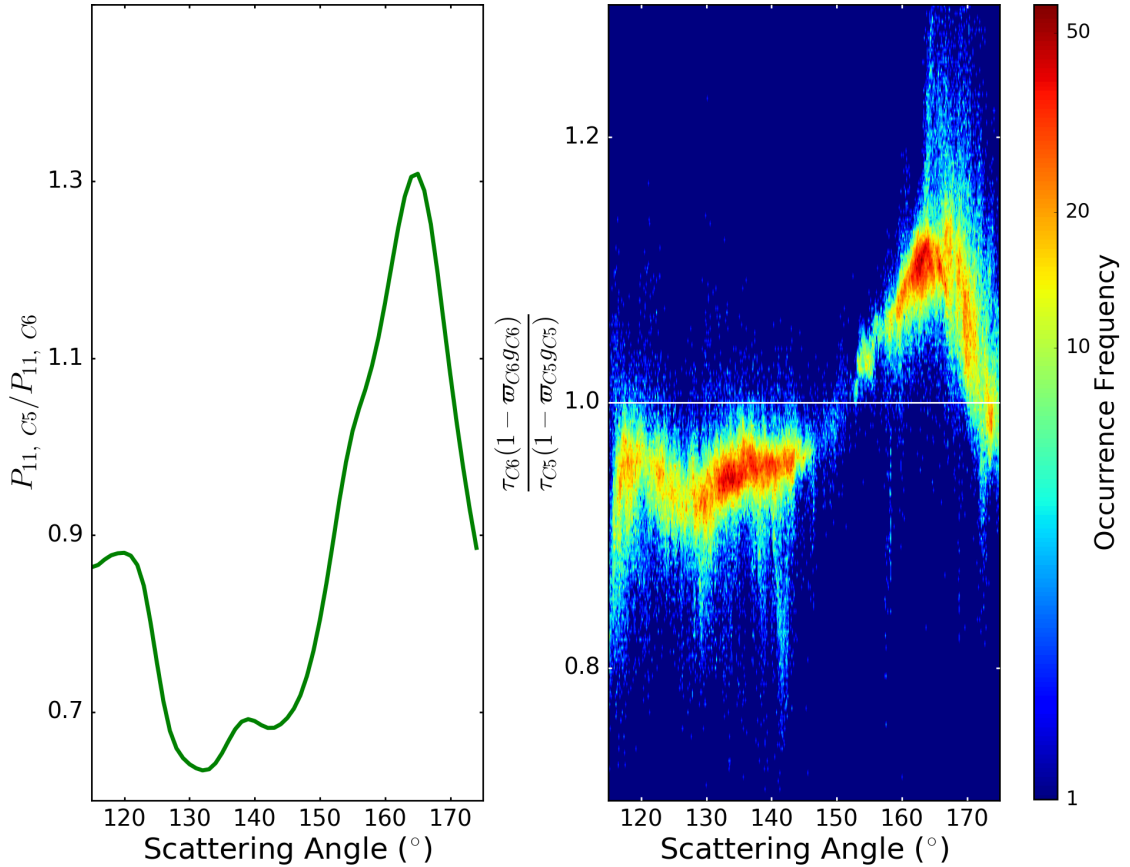


Fig. 11. Left: ratio of C5 and C6 phase function in scattering angle 105° to 165° at $0.86 \mu m$ wavelength with effective radius $30 \mu m$; **Right:** the $\tau(1-\omega g)$ ratio of C6 to C5. The occurrence frequency has a logarithmic scale, and represents the number of data points in each bin.

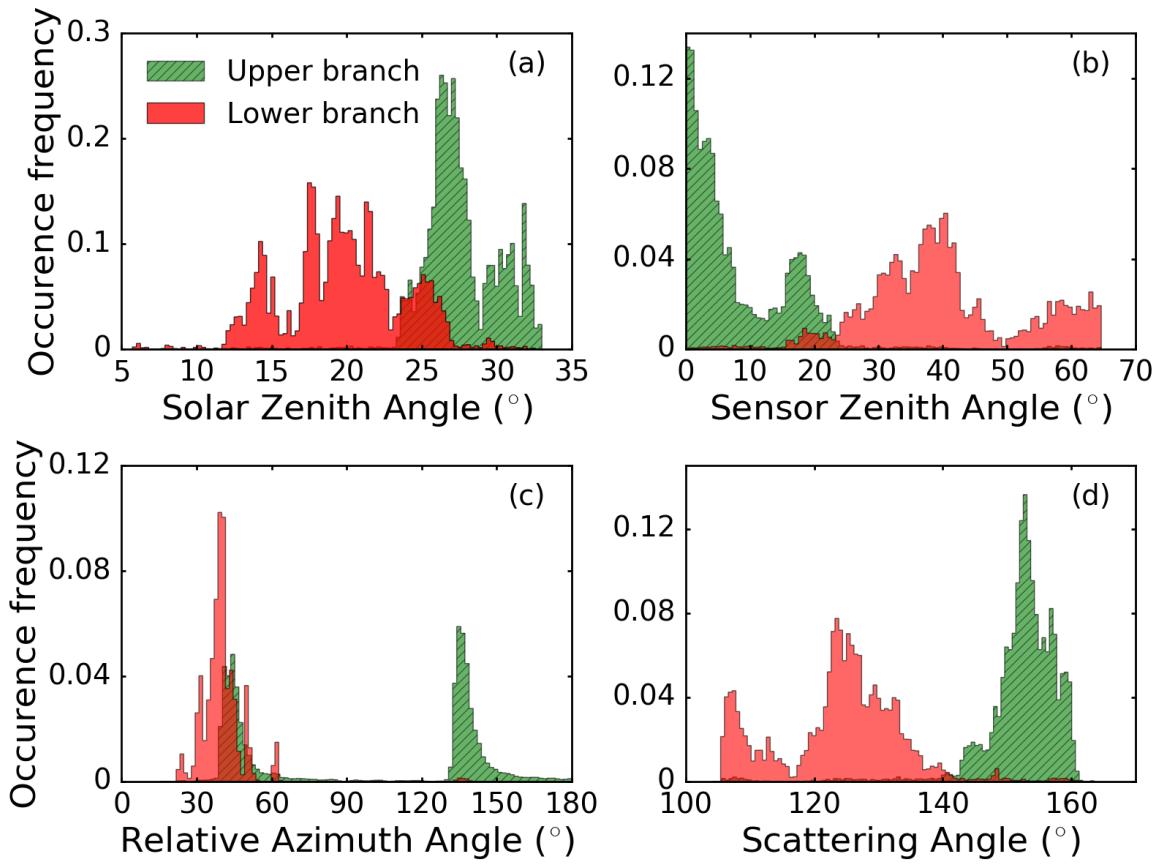


Fig. 12. Viewing geometry and scattering angle distributions of the two data branches shown in Figs. 9 and 10 for effective optical thickness larger than 3. **(a):** solar zenith angle distribution histogram; **(b):** sensor zenith angle distribution histogram; **(c):** relative azimuth angle distribution histogram; **(d):** scattering angle distribution histogram.

In the MODIS cloud product, ice cloud effective radius is retrieved simultaneously together with ice cloud optical thickness. Fig. 13 compares the C5 and C6 ice cloud effective radius retrieval. The C6 ice cloud effective radius retrievals are larger than the C5 counterpart, and they also have a largely linear relationship, though it is not as apparent as in the case of the optical thickness.

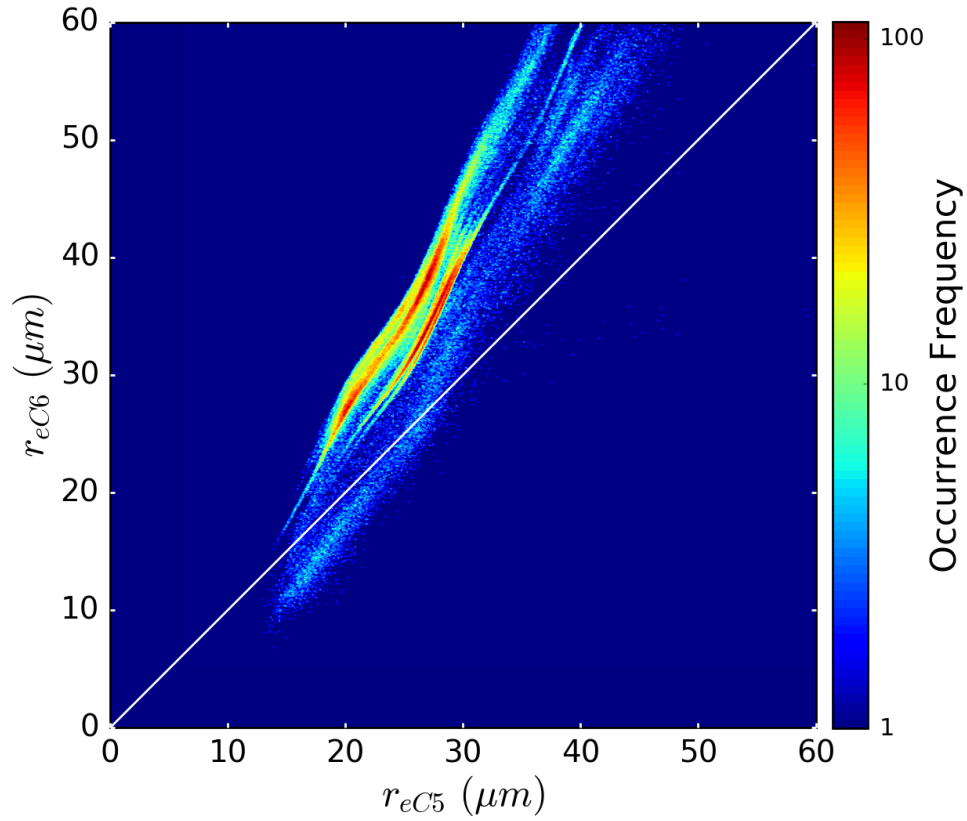


Fig. 13. Comparison of C5 and C6 ice cloud effective radius. The white straight line is the one-to-one ratio line. The occurrence frequency has a logarithmic scale, and represents the number of data points in each bin.

Ice cloud effective radius retrieval is mainly dependent on the absorption band (band 7 here). The similarity parameters in band 7 are derived from the C5 and C6 ϖ and g corresponding to the respective retrieved ice cloud effective radius. The comparison of the similarity parameters is shown in Fig. 14. The distribution of the s values is centered on the one-to-one ratio line. This is consistent with Fig. 7(d), where the same similarity parameters correspond to similar reflectivity in band 7. Fig. 15 shows the similarity parameter s of the C5 and C6 models in band 7 versus effective radius. The same s value corresponds to a larger effective radius of C6 than C5. This is why the MODIS C6 product has larger ice cloud effective radius retrieval than the MODIS C5 counterpart.

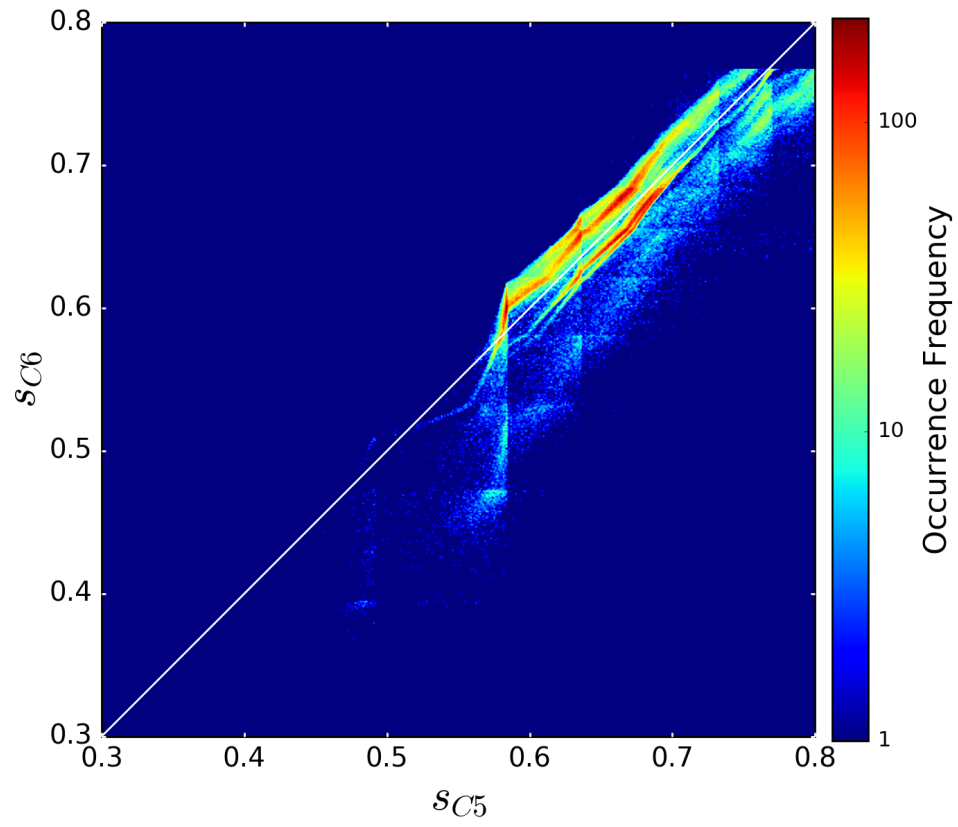


Fig. 14. Comparison of similarity parameter s in MODIS Band 7 derived from the C5 and C6 τ and g corresponding to the respective retrieved ice cloud effective radius. The white straight line is the one-to-one ratio line. The occurrence frequency has a logarithmic scale, and represents the number of data points in each bin.

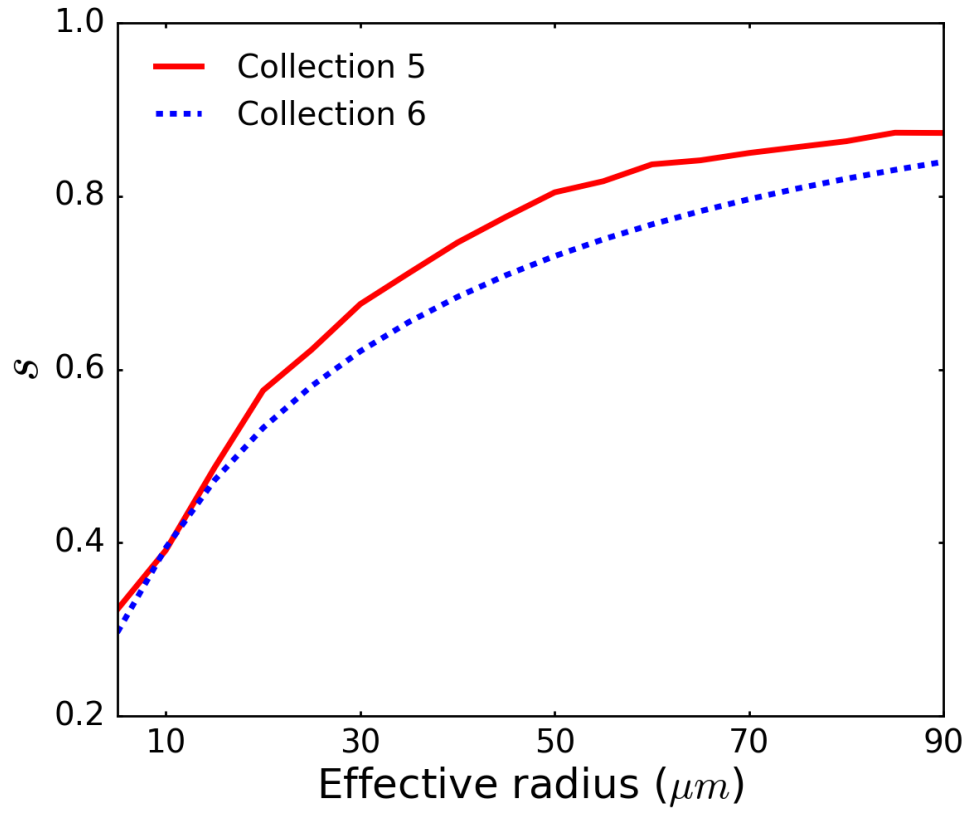


Fig. 15. The similarity parameter s versus effective radius for the C5 and C6 ice cloud models in MODIS bands 7.

Note that the product of r_e and τ is proportional to ice water path (IWP) [31]:

$$\text{IWP} = \frac{4\rho\tau r_e}{3\langle Q_{ext} \rangle}. \quad (13)$$

In Eq. (13), ρ is the density of ice, and $\langle Q_{ext} \rangle$ is the averaged ice cloud particle extinction efficiency defined in the form

$$\langle Q_{ext} \rangle = \frac{\int Q_{ext}(r)A(r)n(r)dr}{\int A(r)n(r)dr}, \quad (14)$$

where $\langle Q_{ext} \rangle$ is approximately 2 because ice particle sizes are much larger than the incident light in visible to near IR bands, A is the ice cloud particle projected area, and n is the particle size distribution.

Fig. 16 shows the comparison between MODIS C5 and C6 IWP datasets. It can be seen that IWP is invariant although the MODIS C5 and C6 optical models are quite different. At present, we are not able to fully comprehend the mechanism in conjunction with the IWP invariant property although we notice that the MODIS C6 product generally has smaller ice cloud optical thicknesses and larger effective radii than the MODIS C5 product (note, $IWP \sim \tau r_e$). Further research is necessary to understand the invariant characteristics of IWP.

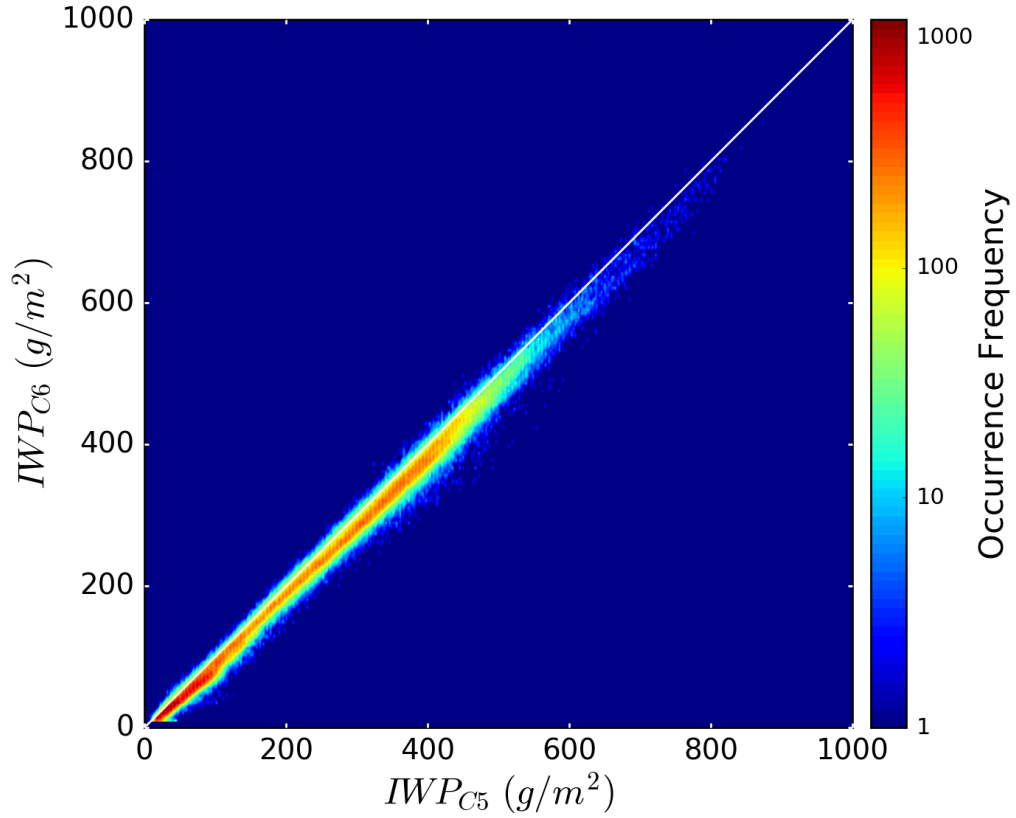


Fig. 16. Comparison of the C5 and C6 ice water path (IWP) data. The white straight line is one-to-one ratio line. The occurrence frequency has a logarithmic scale, and represents the number of data points in each bin.

As pointed out in [17], the principle of similarity for the effective optical thickness in a non-absorbing band can be utilized to estimate ice cloud optical thickness retrievals with a different ice cloud model. For example, the MODIS retrievals with the C6 model are now operational. If there is a new

model that should be evaluated with the same retrieval scheme, one does not need to perform the retrieval, but can just use the quantity $1-g$ in a non-absorbing band of the two models to estimate the new retrieved ice cloud optical thickness from Eq. (3). Ice cloud effective radius retrievals by the new model can also be estimated in a similar way. First, use the C6 ice cloud effective radius data, and C6 ice cloud model single-scattering albedo and asymmetry factor, to get the similarity parameters of the ice cloud pixels. Then one maps the similarity parameters to the new model and obtains the new estimated ice cloud effective radius.

4. Summary and conclusion

In this study, the similarity relations in radiative transfer computations are reviewed and validated for radiance calculations. As McKellar and Box [8] pointed out, the similarity relations given by Eqs. (2) and (3) are approximations of the scaling group of the RTE. In a physical view, Eq. (2) implies that the absorption optical thickness is conserved and Eq. (3) implies that the distribution of scattered light should be roughly consistent. For conservative scattering, both sides of Eq. (2) are zero so that the two conditions can be satisfied for two different phase functions only by scaling optical thickness, whereas for non-conservative scattering, both single-scattering albedo and optical thickness should be scaled. The similarity parameter defined in Eq. (12) combines Eqs. (2) and (3), and is a similarity condition for non-conservative scattering.

The DISORT radiative transfer model is implemented with 256 streams to calculate reflectance and transmittance of a single layer ice cloud with the C5 and C6 ice cloud models by keeping Eqs. (2) and (3) invariant. Results show that both reflectance and transmittance are similar for the two MODIS ice cloud models in bands 2 and 7. Furthermore, the similarity also depends on the optical thickness. The results of the two ice cloud models become closer when optical thickness increases and tend to an asymptotic value. With a large optical thickness, the reflectance of the C5 and C6 models is nearly isotropic in band 2 but not in band 7. According to the physical mechanism of multiple scattering, high-order scattering that is more

isotropic significantly contributes to reflectance in a non-absorbing band, whereas the reflectance in an absorbing band is mainly determined by low-order scattering that is anisotropic. In addition, ice cloud reflectivity is simulated in bands 2 and 7 with random MODIS viewing geometry and optical thickness based on the C5 and C6 models. In band 2, if the optical thickness is invariant, C6 reflectivity is larger than C5 whereas if the effective thickness is invariant, the C5 and C6 reflectivities are nearly identical. In band 7, if Eqs. (2) and (3) are satisfied concurrently, which implies that the similarity parameter is conserved, the C5 and C6 reflectivity values are nearly identical.

To further investigate the similarity relation and its effect on remote sensing, we analyze the similarity between the operationally retrieved ice cloud optical thickness and effective radius using MODIS C5 and C6 Level 2 cloud property datasets. The C6 ice cloud optical thickness is smaller than C5, and they have roughly a linear correlation between them. In contrast, the effective optical thicknesses $\tau(1-\omega_g)$ in band 2 are similar for the C5 and C6 datasets, and their ratio is around one with some broadening. The C6/C5 $\tau(1-\omega_g)$ ratio is also a function of scattering angle, and its variation has nearly the same pattern as the C5/C6 phase function ratio. This suggests a stricter similarity relation than Eq. (3). If the two optical thicknesses have a relation with similar angular dependence, the radiative transfer calculation results can be the same. The angle-dependent relation should be related to the phase functions.

The similarity parameters in band 7 are derived from the C5 and C6 single-scattering albedo and asymmetry factor corresponding to their respective retrieved ice cloud effective radius. Though their ice cloud effective radii are significantly different, the derived similarity parameters are similar. Since the C6 model has a smaller s than the C5 model in band 7 at the same size, the C6 ice cloud effective radius is larger than the C5 counterpart. Because of the similar scales of the C5 and C6 ice cloud optical thickness and effective radius differences, the corresponding IWP retrievals are nearly identical. Furthermore, the similarities of $\tau(1-\omega_g)$ and s can be utilized to estimate the retrieved cloud optical thickness and effective radius if using a new ice cloud model. As such, ice scattering properties as a function of effective size are provided in the C6 MOD06 file for all relevant spectral bands used in the retrievals, allowing for scaling to

user-specific ice radiative models.

Acknowledgments

This paper is supported by NASA (NNX15AG66G) and partly by the Hagler Institute for Advanced Study at Texas A&M University Heep Graduate Fellowship.

References

- [1] van de Hulst HC, Grossman K. Multiple light scattering in planetary atmospheres. In: Brandt JC, McElroy MB, editors. *The Atmospheres of Venus and Mars*. New York, NY: Gordon and Breach Science Publishers Inc: 1968, p. 35–55.
- [2] van de Hulst HC. Multiple scattering in planetary atmospheres. *J Quant Spectrosc Radiat Transf* 1971;11:785–95.
- [3] van de Hulst HC. Some problems of anisotropic scattering in planetary atmospheres. In: Sagan, C, Owen, TC, Smith HJ, editors. *Planetary Atmospheres*. Dordrecht, Holland: D Reidel Publishing Co: 1971, p. 177–85.
- [4] van de Hulst HC. The spherical albedo of a planet covered with a homogeneous cloud layer. *Astron Astrophys* 1974;35:209–14.
- [5] Hansen JE. Absorption-line formation in a scattering planetary atmosphere: A test of van de Hulst’s similarity relations. *Astrophys J* 1969;158:337–49.
- [6] Hunt GE. A review of computational techniques for analysing the transfer of radiation through a model cloudy atmosphere. *J Quant Spectrosc Radiat Transf* 1971;11:655–90.
- [7] Irvine WM. Multiple scattering in planetary atmospheres. *Icarus* 1975;25:175–204.
- [8] McKellar BH, Box MA. The scaling group of the radiative transfer equation. *J Atmos Sci* 1981;38:1063–8.

- [9] Mitrescu C, Stephens GL. On similarity and scaling of the radiative transfer equation. *J Quant Spectrosc Radiat Transf* 2004;86:387–94.
- [10] Rozanov VV, Lyapustin AI. Similarity of radiative transfer equation: Error analysis of phase function truncation techniques. *J Quant Spectrosc Radiat Transf* 2010;111:1964–79.
- [11] Mishchenko MI, Travis LD, Lacis AA. Multiple scattering of light by particles: radiative transfer and coherent backscattering. Cambridge, UK: Cambridge University Press; 2006.
- [12] Sobolev VV. Light scattering in planetary atmospheres. Oxford: Pergamon Press; 1975 Section 8.
- [13] Chandrasekhar S. Problems with general laws of scattering. New York, NY: Dover; Radiative Transfer 1960, p. 127–60.
- [14] Liou KN. An Introduction to Atmospheric Radiation. San Diego, CA: Academic Press; 2002.
- [15] Joseph JH, Wiscombe WJ, Weinman JA. The delta-Eddington approximation for radiative flux transfer. *J Atmos Sci* 1976;33:2452–9.
- [16] Twomey S, Bohren CF. Simple approximations for calculations of absorption in clouds. *J Atmos Sci* 1980;37:2086–95.
- [17] Platnick S, Meyer K, King MD, Wind G, Amarasinghe N, Marchant B, Arnold GT, Zhang Z, Hubanks PA, Holz RE, Yang P, Ridgway WL, Riedi J. The MODIS cloud optical and microphysical products: updates for Collection 6 and examples from Terra and Aqua. *IEEE Trans Geosci Remote Sens* 2017;55:502–25.
- [18] Wiscombe WJ. The delta-M method: rapid yet accurate radiative flux calculations for strongly asymmetric phase functions. *J Atmos Sci* 1977;34:1408–22.
- [19] King MD. A method for determining the single scattering albedo of clouds through observation of the internal scattered radiation field. *J Atmos Sci* 1981;38:2031–44.
- [20] King MD, Harshvardhan. Comparative accuracy of selected multiple scattering approximations. *J Atmos Sci* 1986;43:784–801.

- [21] Iwabuchi H. Efficient Monte Carlo methods for radiative transfer modeling. *J Atmos Sci* 2006;63:2324-39.
- [22] Cahalan RF, Oreopoulos L, Marshak A, Evans KF, Davis AB, Pincus R, et al. The 13RC: Bringing together the most advanced radiative transfer tools for cloudy atmospheres. *Bull Amer Meteor Soc* 2005;86:1275–93.
- [23] Stamnes K, Tsay SC, Wiscombe W, Jayaweera K. Numerically stable algorithm for discrete-ordinate-method radiative transfer in multiple scattering and emitting layered media. *Appl Opt* 1988;27:2502–9.
- [24] Baum BA, Heymsfield AJ, Yang P, Bedka ST. Bulk scattering properties for the remote sensing of ice clouds. Part I: Microphysical data and models. *J Appl Meteor* 2005;44:1885–95.
- [25] Holz RE, Platnick S, Meyer K, Vaughan M, Heidinger A, Yang P, Wind G, Dutcher S, Ackerman S, Amarasinghe N, Nagle F, Wang C. Resolving ice cloud optical thickness biases between CALIOP and MODIS using infrared retrievals. *Atmos Chem Phys* 2016;16:5075–90.
- [26] Nakajima T, Tanaka M. Algorithms for radiative intensity calculations in moderately thick atmospheres using a truncation approximation. *J Quant Spectrosc Radiat Transf* 1988;40:51–69.
- [27] Hioki S, Yang P, Kattawar GW, Hu Y. Truncation of the scattering phase matrix for vector radiative transfer simulation. *J Quant Spectrosc Radiat Transf* 2016;183:70–7.
- [28] Nakajima T, King MD. Determination of the optical thickness and effective particle radius of clouds from reflected solar radiation measurements. Part I: Theory. *J Atmos Sci* 1990;47:1878–93.
- [29] Sun J, Angal A, Xiong X, Chen H, Geng X, Wu A, et al. MODIS reflective solar bands calibration improvements in Collection 6. *Proc SPIE* 2012;8528:1–10.
- [30] Platnick S, Ackerman SA, King MD, Meyer K, Menzel WP, Holz RE, Baum BA, Yang P. MODIS atmosphere L2 cloud product (06_L2). NASA MODIS Adaptive Processing System, Goddard Space Flight Center 2015: [dx.doi.org/10.5067/MODIS/MYD06_L2.006](https://doi.org/10.5067/MODIS/MYD06_L2.006).

- [31] Yang P, Tsay SC, Wei H, Guo G, Ji Q. Remote sensing of cirrus optical and microphysical properties from ground-based infrared radiometric measurements-part I: a new retrieval method based on microwindow spectral signature. *IEEE Geosci Remote Sens Lett* 2005;2:128–31.